

A Validated Numerical-Experimental Design Methodology for a Movable Supersonic Ejector Compressor for Waste Heat Recovery

Sajad Alimohammadi^{1*}, Tim Persoons¹, Darina B. Murray¹, Mohamadreza S. Tehrani², Bijan Farhanieh²,
Juergen Koehler³

¹ Department of Mechanical and Manufacturing Engineering, Trinity College, Dublin 2, Ireland
(* Corresponding author. E-mail: alimohas@tcd.ie, Phone: +353 1 896 1998)

² School of Mechanical Engineering, Sharif University of Technology, Tehran, Iran

³ Institute for Thermodynamics, Technical University of Braunschweig, Braunschweig, Germany

Abstract

The aim of this paper is to develop the technical knowledge, especially the optimum geometries, for the design and manufacturing of a supersonic gas-gas ejector for a waste heat driven vehicle cooling system. Although several studies have been performed to investigate the effects of geometrical configurations of gas-gas ejectors, a progressive design methodology of an ejector compressor for application to a vehicle cooling system has not yet been described. First, an analytical model for calculation of the ejector optimum geometry for a wide range of operating conditions is developed, using R134a as the working fluid with a rated cooling capacity of 2.5 kW. The maximum values of entrainment ratio (ω) have been estimated by correlation of the main parameters in a non-dimensional form. The optimum values of nozzle throat diameter (d_{nt}) and mixing chamber diameter (d_{mc}) thus obtained are used as a starting point for the CFD optimization covering a wide range of geometrical configurations. To assess the effect of various dimensional quantities, an optimization technique has been proposed for calculation of the most efficient geometry of the target ejector for manufacturing. Using a vehicle cooling system as a test case, the final optimized dimensions are reported and discussed. An experimental validation confirms the CFD results and the ejector performance with a normalized deviation of 5% between observed and simulated results, demonstrating that the methodology is a valid ejector design tool for a wide range of applications.

Keywords

Ejector; Vehicle Cooling; CFD; Experimental Validation; Design Methodology; Supersonic Flow; Waste Heat Recuperation

Nomenclature

d	Diameter, m
l	Length, m
\dot{m}	Mass flow rate, kg/s
P	Static pressure, kPa
T	Static temperature, °C

Greek letters

φ	Area ratio
Ψ	Compression ratio
ξ	Driving pressure ratio
ω	Entrainment ratio

Subscripts

c	Condenser
d	Diffuser
e	Evaporator
g	Generator (Heat exchanger)
M	Mixed flow conditions at the outlet of ejector (downstream)
mc	Mixing chamber
ne	Nozzle exit
nt	Nozzle throat
p	Primary flow
s	Secondary flow

Abbreviations

CFD	Computational fluid dynamics
COP	Coefficient of performance
NEP	Nozzle exit position

1 Introduction

Thermal energy is widely available as a byproduct in many applications such as vehicle engines, industrial processes, geothermal activities and solar power generation. Operational usage of this energy is beneficial from environmental and economic points of view. Among the various techniques, one useful approach is using this energy to meet a cooling demand by means of an ejector refrigeration system. Replacing a conventional vehicle cooling system with a waste heat driven ejector refrigeration system was

the goal of a previous study by some of the authors [1]. In the conventional vapor-compression refrigeration system, the compressor is driven by the engine crankshaft via a belt. This reduces the effective engine output power, and the compressor introduces noise and vibration.

In an ejector-driven system (Fig. 1), the energy needed to compress the refrigerant from the evaporator into the condenser can be provided by waste heat from the vehicle coolant loop. The system combines a Rankine power cycle and a refrigeration cycle, where a gas-gas ejector replaces the compressor of the refrigeration cycle and the turbine of the power cycle. As shown in Fig. 1(a), the working fluid is vaporized in the heat exchanger. The primary motive flow enters the ejector (1) as a high pressure and high temperature gas which expands through the primary convergent-divergent nozzle, accelerating to supersonic speeds. At the primary nozzle exit, the subpressure entrains low pressure refrigerant vapor from the evaporator as an secondary flow. Both flows merge in the ejector mixing chamber, recovering pressure by converting kinetic energy to pressure energy while flowing through the diffuser (3). Thereafter, the vapor enters the air cooled condenser where heat is rejected to the ambient. The liquid refrigerant leaving the condenser (4) partly flows through an expansion valve to the evaporator (5) where the lower pressure liquid refrigerant is vaporized by absorbing heat from the passenger compartment (2), and partly flows back to the heat exchanger through a pump to close the cycle (6).

At the heart of the cycle, the optimum design of the ejector is critical for the coefficient of performance (COP). Due to the highly complex flow inside the ejector, the main challenge is to develop a methodology for designing a supersonic ejector for use in these applications. To ensure sufficient accuracy in the design, a combination of computational fluid dynamics (CFD) and experimental validation is required. As a key CFD study of gas-gas ejectors for refrigeration applications, Riffat and Everitt [2] have shown the effect of ejector nozzle type and position on its performance. In transonic compressible flows involving shock waves and shear mixing layer interaction, the choice of the turbulence model and grid refinements are crucial. The influence of six well-known turbulence models has been studied by Bartosiewicz et al. [3]. Sriveerakul et al. [4] have revealed the complex nature of the mixing process of a steam ejector used in a jet refrigeration cycle. Their CFD results show that the realizable k-epsilon model agrees reasonably well with experimental data. Khalil et al. [5] have developed a model to design R134a ejectors for waste heat recovery applications. Their results confirm that adequate operation of ejector refrigeration systems for air-conditioning can be achieved with waste heat source temperatures from 65°C to 85°C, which partly overlaps with the vehicle coolant system temperature range. The effects of different nozzle structures on the performance of a steam ejector have been investigated numerically by Yang et al [6]. Aphornratana and Eames [7] have experimentally shown the benefit of using a movable primary nozzle in the ejector to maximize the performance in off-design operating conditions by adjusting the nozzle exit position (NEP). Lucas and Koehler ([8]-[10]) have experimentally achieved a 17% improvement in COP using an ejector in

a CO₂ expansion valve refrigeration cycle. They have proposed useful correlations for the ejector efficiency and the driving mass flow rate. Only a few studies have looked at the performance of ejector refrigeration systems for vehicle air conditioning using energy recovery from the vehicle coolant system (e.g., Rogdakis et al. [11], Huang et al.[12]). Al-Khalidy and Zayonia [13] experimented on an ejector in an air conditioning system with R113 as working fluid. For a generating temperature of 100.7 °C, condensing temperature of 44 °C and an evaporating temperature of 5.5 °C, they obtained a COP = 0.26.

Although a few studies have been performed to investigate the effects of geometrical configurations of gas-gas ejectors, a systematic ejector design methodology for the specific application of a vehicle cooling system has not yet been described. The present work outlines such a methodology, and identifies and discusses the optimum geometries for design and manufacturing of supersonic ejectors. Most studies reported ejector performance as a function of dimensional parameters (e.g., Hewedy et al. [14], Kim and Kwon [15], Boumaraf and Lallemand [16], Li et al. [17]). In this paper, an optimization technique is presented based on the three main geometrical values as dimensionless parameters.

2 Ejector Design Methodology

The design methodology comprises three steps: 1-D analytical modeling, CFD simulation, and experimental validation of the numerical approach.

2.1 First step: 1-D Analytical Modeling

A basic one-dimensional analytical model for calculation of the optimum ejector geometry for a wide range of operating conditions is derived by solving a set of coupled differential equations representing the conservation of mass, momentum, and energy at 5 characteristic locations within the ejector. As shown in Fig. 1(b), these locations are: (1) nozzle throat and (2) exit, (3) mixing chamber inlet section, (4) hypothetical shock section and (5) diffuser inlet section. These are the only points in which the state variables are solved using the 1-D formulation, similar to the approach described in greater detail by Alimohamadi et al. [1]. This model requires the physical properties of the working fluid (R134a) and iterative computations, which are solved using a computer code. Section 3.1 discusses the effects of four main parameters, namely area ratio and temperatures in the generator, condenser and evaporator, on both ejector entrainment ratio (ω) and COP. Also, the maximum value of ω has been estimated by correlation of effective parameters in a dimensionless form.

Four characteristic parameters for ejectors are defined here. The entrainment ratio, defined as mass flow rate of secondary flow, m_s , to mass flow rate of primary flow, m_p ,

$$\omega = \frac{m_s}{m_p} \quad (1)$$

The area ratio, defined as the cross-sectional area of the mixing section to the nozzle throat area,

$$\varphi = \frac{A_{mc}}{A_{nt}} \quad (2)$$

The compression ratio, defined as the pressure of mixed flow at the outlet (downstream) of the ejector to the inlet pressure of the secondary flow,

$$\Psi = \frac{P_M}{P_s} \quad (3)$$

The driving pressure ratio, defined as the pressure of primary flow to the pressure of mixed flow at the outlet of ejector,

$$\xi = \frac{P_p}{P_M} \quad (4)$$

The primary and secondary fluids at the inlets and the mixed fluid at the exit of the ejector are assumed to be at stagnation conditions, and the quantities P_s , P_p and P_M represent the pressures in the evaporator (P_e), heat exchanger (P_g), and condenser (P_c), respectively.

The optimum ejector dimensions determined using the 1-D analytical model are merely used as the starting point configuration for the three-dimensional CFD simulation described in the following section. This was found to ensure better convergence of the CFD optimization (see sections 3.2.2 and 3.2.3).

2.2 Second Step: CFD simulation

The commercial CFD package Fluent is used to evaluate the flow in the ejector on the basis of the conservation laws for compressible fluid flow, using the k-epsilon Realizable turbulence model as closure. Using the solution of the 1-D analytical model as a starting point, a parametric study of all relevant dimensions (diameters, lengths, angle of convergence-divergence, etc.) has been carried out, as discussed in Sect. 3.2.2.

2.2.1 Pre-Processing: Geometry of Solution Domain

Based on the 1-D analytical model solution, a preliminary model for the ejector is shown in Fig. 2. These dimensions are subject to variation in the dimensional analysis of the ejector. Except for the intake portion of secondary flow to the ejector, an assumption of axisymmetric flow inside the ejector provides a

good approximation, as will be demonstrated by the experimental validation results in Sect. 2.3. This has considerably reduced the time needed to achieve a satisfactory convergence.

2.2.2 Pre-Processing: Grid Generation

Discretization of the solution domain is a critical step in the modeling procedure. The order of precision for the numerical solution is highly dependent on mesh quality and the total number of cells, with increasing cell density usually resulting in a more accurate solution, at the expense of an increase in solution time. A discretized domain has been generated using about 40,000 structured quadratic cells, as depicted in Fig. 2. To increase the solution accuracy and optimize convergence in the presence of high velocity gradient regions, two advanced methods referred to as *adaptive grid* and *adaptive boundary* have been used. Thus, the mesh is relatively sparse for low velocity regions, and denser for high velocity gradient regions such as the primary nozzle jet core, ejector wall, and the region of interaction between entrained and motive flows (see Fig. 2).

2.2.3 Flow Physics and Boundary Conditions

The physical model used here is steady, viscous, adiabatic, turbulent, and compressible. With the exception of vapor phase density which is evaluated by the ideal gas law, the other physical properties (i.e., specific heat capacity, dynamic viscosity and thermal conductivity) are averaged using the real gas properties of R134a as the working fluid at the five locations along the ejector length (see Sect. 2.1) and assigned in the material library of the Fluent model.

As boundary conditions, two inlet pressure and one exit pressure boundaries are defined at saturated conditions. The turbulent boundary condition has been determined using the hydraulic diameter and turbulence intensity which is fixed at between 2 to 3%. This is due to low speed flow being treated as a medium-turbulence case in both inlet sections and also the exit section.

2.3 Third step: Experimental Validation of the CFD Approach

An experimental validation setup is designed using nitrogen and ambient air as working fluids, with the aim of verifying the operation of the ejector and validating the CFD approach. The setup consists of (i) a low and high pressure tank on a mass balance, (ii) the supersonic ejector with a design similar to Fig. 2, (iii) a flow meter, pressure gauges and fluidic connections. The low pressure tank (initially at atmospheric pressure) is charged with a quantity of ambient air entrained through the ejector as secondary flow, while pressurized nitrogen acts as the motive flow. The ejector entrainment port is free to ambient air via a flow meter, and the primary flow inlet is connected to a high pressure nitrogen tank. The primary mass flow rate is calculated by recording the time and mass of the high pressure tank. In starting the test, the high pressure

nitrogen flows to the primary nozzle, entraining the air inside the ejector. As a result, the low pressure tank is charged to a pressure above atmospheric. Charging continues until an equilibrium pressure is reached in the low pressure tank, depending on the adjusted upstream pressure of the primary inlet flow. To ensure a quasi-steady state is reached, each step is started from atmospheric pressure inside the low pressure tank for different high pressures, thereby canceling the overlapping effect of steps on each other. The repeatability is within 2% of the equilibrium pressure. The total measurement time is 5 minutes, with measurements taken after a quasi-steady state has been reached with fluctuations in pressure within 2% of the constant value.

The experimental results in Table 1 are recorded at the incipience of reverse flow inside the ejector, which corresponds to the highest possible charging pressure (equilibrium pressure) in the low pressure tank. Conversely, the exact conditions of this experiment are simulated with the developed CFD ejector model to serve as a validation of the numerical simulation procedure. The model now uses nitrogen as working fluid (instead of R134a which is used for the main results in Sect. 3.2). As an example, Mach contours are shown in Fig. 3 for a fixed upstream pressure of 27.5 bar. By stepwise increasing the downstream pressure, reverse flow occurs at a downstream pressure of 5.2 bar. This indicates the maximum achievable pressure in the low pressure tank for an upstream pressure of 27.5 bar. The same comparison is repeated for the other experimental conditions. The numerical and experimental results are in excellent agreement with a normalized deviation around 5%. This confirms that the aforementioned CFD methodology can be used as an ejector design methodology for this type of application.

3 Simulation Results and Discussion

3.1 1-D Analytical Modeling Results

The 1-D simulation results are discussed in terms of the entrainment ratio as a function of operating conditions and ejector geometry. The working fluid is R134a with a rated cooling capacity of 2.5 kW, representative of a typical passenger car air-conditioning system.

3.1.1 Design Study

For the optimum ejector geometry, the value of area ratio should be estimated at maximum value of entrainment ratio (Fig. 4). As shown in Fig. 4, the curves for different evaporator temperatures have almost the same area ratio for the maximum entrainment ratio, i.e., an approximate area ratio of 4.2. For a fixed area ratio, the entrainment ratio increases with increasing evaporator temperature, which can be explained as follows: the kinetic energy of the primary flow at the nozzle exit serves on the one hand to draw in the secondary flow and on the other hand to compress the mixed flow to the diffuser pressure. For fixed geometry and defined operating conditions, an increase of the evaporator temperature reduces the compression ratio, Ψ . This means that only a small part of the available kinetic energy of the primary flow

is used for the pressure increase between the evaporator and the diffuser. The rest of the kinetic energy induces the secondary flow into the mixing chamber, and thus the entrainment ratio increases.

According to Fig. 4, the maximum entrainment ratio increases for higher generator temperatures and lower condenser temperatures. Similarly, the optimal area ratio also increases. The optimal configuration of ejector geometry, as the starting point for the CFD simulation is taken as

$$d_{nt} = 3 \text{ mm}, d_{ne} = 5 \text{ mm}, \text{ and } d_{mc} = 7 \text{ mm} \quad (5)$$

The procedure for selecting this initial configuration is described in greater detail in Alimohamadi et al. [1]. The relations between nozzle throat, nozzle exit and mixing chamber diameters are derived as a function of physical properties using conservation laws and fluid dynamics principles within the ejector. For the chosen automotive refrigeration test case with average saturated temperatures of the primary flow (generator) at 85°C, secondary flow (evaporator) at 5°C, and mixed flow (condenser) at 40°C, the area ratio is optimized using the constant temperatures lines in Fig. 4. Then using the ratio of nozzle throat and exit diameters, the above values are calculated. As described in Sect. 3.2, the parameters in Eq. (5) are further optimized to achieve higher accuracy results using CFD.

3.1.2 Off-Design Study

For the given ejector geometry (Sect. 3.1.1), the effect of off-design operating conditions on the ejector performance has been investigated. In Fig. 5, the performance is characterized by the entrainment ratio as a function of the main dimensionless parameters in Eqs. (2-4): compression ratio, driving pressure ratio, and area ratio. The correlations in Eqs. (6) and (7) are least square fitted to the simulated entrainment ratio values with coefficient of determination values $R^2 > 0.7$.

$$\omega = 0.0603(\Psi)^3 + 21.43(\xi)^3 - 0.1073(\Psi)^2(\xi) - 0.7743(\Psi)(\xi)^2 - 0.2673(\Psi)^2 - 164.6(\xi)^2 + 4.753(\Psi)(\xi) - 5.635(\Psi) + 419.9(\xi) - 365.5 \quad (6)$$

and

$$\omega = -0.0803(\varphi)^3 - 1.78(\Psi)^3 - 0.3181(\varphi)^2(\Psi) + 0.0149(\varphi)(\Psi)^2 + 1.559(\varphi)^2 + 14.17(\Psi)^2 + 2.659(\varphi)(\Psi) - 9.016(\varphi) - 43.59(\Psi) + 50.62 \quad (7)$$

The above formulations allow to predict the optimum design parameters corresponding to a maximum value of the entrainment ratio ω . Despite the convenience of these analytical results, it is inherently incapable of incorporating multi-dimensional phenomena such as oblique shocks and shock-induced boundary layer separation (Al-Ansary [18]).

3.2 CFD Simulation Results

3.2.1 Flow Pattern within the Ejector

In the primary nozzle, the high pressure and temperature flow accelerates and expands leading to choked flow at the throat section, and undergoes a further acceleration in the expanding section. At the nozzle exit, the primary flow still has a higher pressure than the surrounding fluid inside the mixing chamber. Its residual depressurization results in expansion waves at the nozzle exit, as shown in Fig. 6(a). Due to the pressure difference between the primary and secondary flows, a first series of oblique shock waves occurs along the mixing layer with a noticeable expansion angle. This behavior can also be observed from the pressure distribution along the ejector length, shown in Fig. 6(b). As the primary and secondary flows combine into the convergent section of the mixing chamber, the shear mixing layer causes an acceleration of the surrounding secondary flow. In turn, this viscous-shear momentum exchange reduces the momentum of the primary supersonic jet core, which is shown by the diminishing fluctuating oscillations in the pressure distribution along the ejector length in Fig. 6(b). At a certain section inside the mixing chamber, the total velocity reaches sonic speed and chokes. The effective area of secondary choked flow at this section can be calculated by estimation of the annular area between the ejector wall and primary core flow. Finally, in a section between the end of the mixing chamber and the inlet to the diffuser, a second series of oblique shock waves occurs, which results in an increase of static pressure and fully subsonic flow at the diffuser inlet; the shock waves diminish until the end of mixing chamber, and the static pressure of the subsonic flow recovers inside the diverging section of the diffuser (see Fig. 6(b)).

To achieve a better understanding of the complex flow inside the ejector, the effect of operating conditions and dimensions is discussed in the following section (Sect. 3.2.2), leading to the determination of the optimal geometry for the target waste-heat driven refrigeration system (Sect. 3.2.3).

3.2.2 Effect of Ejector Geometry

The effect of ejector geometry on its performance is discussed in three sections: (1) the primary nozzle, (2) the mixing chamber, and (3) the diffuser. In each case, only one dimension is changed, keeping all others constant. The fixed operating conditions are representative of a vehicle air-conditioning system: saturated temperatures of primary and secondary flows at 85 °C ($P_p = 25.26$ bar) and 5 °C ($P_s = 3.496$ bar), respectively, using R134a as working fluid. To study the effect of different flow phenomena inside the ejector (e.g., single and double choked flow, the location of shock waves and the variation of shock wave intensity) a range of downstream saturated temperatures have been investigated (from $T = 8.87$ °C, $P = 4$ bar to $T = 45$ °C, $P = 11.6$ bar).

3.2.2.1 Effect of the primary nozzle geometry

The design of the primary nozzle is crucial as it performs one of the main functions of the ejector. Kim et al. [19] have evaluated ejector performance by changing the throat area for a vacuum pump application. In this study, the effect of its geometry has been examined in terms of (i) the throat diameter (d_{nt}), (ii) the nozzle exit diameter (d_{ne}), and (iii) the nozzle exit position (NEP) in the mixing chamber.

The effect of the nozzle throat diameter on the entrainment ratio is shown in Fig. 7(a). Huang et al. [20] have shown that choked flow can occur in two locations: in the throat section of the primary nozzle and in the mixing chamber. The latter occurs when the entrained flow accelerates from a low velocity state at the suction port to a sonic flow in the constant area section of the mixing chamber. This behavior is confirmed by Fig. 7(a). Double choked flow occurs when the downstream pressure is lower than a critical value which is unique to a given geometry and operating conditions. In this regime, the entrainment ratio becomes independent of downstream pressure and the ejector is working at its maximum performance, as represented by the horizontal trend lines in Fig. 7(a). By contrast, single choked flow occurs by increasing the back pressure to the values above the critical pressure, causing a sudden drop of entrainment ratio to much lower values, as represented by the downward trend lines in Fig. 7(a). In this latter mode only the flow in the primary nozzle is choked and the ejector is working below its optimum capacity. An even greater rise in back pressure further deteriorates the performance with entrainment ratio approaching zero, corresponding to the incipience of reverse flow in the ejector (Sect. 2.3). Figure 7(a) shows that reducing the throat diameter increases the entrainment ratio, but the back pressure should be reduced to maintain the double choked flow regime inside the ejector, which ensures optimum operation. This counteracting effect should be kept in mind in the design of the primary nozzle.

The procedure to find the critical points in Fig. 7(a) consists of finding the intersection of the horizontal (i.e., constant entrainment ratio) and downward (single choked flow regime) trends. Due to the non-linear nature of the ejector performance, these represent fitted lines through a number of operating points. Especially the downward trend line requires several points to be determined accurately. After obtaining the approximate value of the critical point for each specific operating condition, some additional simulations are performed at downstream pressures close to this value to refine and find the final intersection. As shown in Fig. 7(a), the simulations are mainly concentrated close to the critical point and over the downwards trend. The same technique is applied in Figs. 8, 10.

Figure 7(b) illustrates the variation of the static pressure along the centerline of the ejector for the same cases as Fig. 7(a). By increasing the diameter of the nozzle throat section, the momentum of the primary and mixed flow increases. This intensifies the second series of oblique shock waves as the peak of each wave moves toward the end of mixing chamber (Fig. 7(b)). Consequently, the pressure enhancement due to these waves rises, which helps to increase the upper limit for the critical back pressure at the exit of diffuser, as the ejector stays in double choked mode (Fig. 7(a)).

Figure 7(b) also shows the displacement of the peak of the first series of oblique shock waves towards the inlet of the mixing chamber, as the nozzle throat diameter increases. Due to the higher pressure and momentum of the supersonic primary jet core, compared to the surrounding subsonic entrained flow at the inlet of mixing chamber, the jet core first expands to lower pressures than that of surrounding flow and subsequently compresses to higher pressure. This phenomenon repeats in an oscillatory manner in a series of shock waves. As decreasing the throat diameter results in the formation of a more powerful primary jet core with higher momentum and pressure, the peak of the waves moves toward the left and the shock wave propagates to a larger downstream distance before equalizing out.

The effect of the nozzle exit diameter on ejector performance is shown in Fig. 8(a). By increasing the nozzle diameter, the entrainment ratio drops. The variation of nozzle exit size does not have a significant effect on the primary mass flow rate. As the primary flow passes the nozzle throat, the supersonic flow expands in the diverging section. At the nozzle exit, due to higher pressure difference between the surrounding flow and the jet core, the expansion continues. An increase in nozzle exit diameter leads to a larger expansion angle and reduces the entrained flow rate. An exact relationship for the variation of critical back pressure was not derived from the results. However, as the nozzle exit diameter increases from 4 mm to 5 mm, the critical back pressure rises and subsequently drops for a nozzle exit diameter of 6 mm. The final value for this dimension should be selected using an optimization process which runs the ejector in an acceptable range for both the critical back pressure and the entrainment ratio. Figure 8(b) shows the static pressure along the center line of the ejector for different primary nozzle exit diameters. A more pronounced pressure oscillation of the first series of shock waves at the outlet section of primary nozzle can be seen for a nozzle exit diameter of 6 mm. The shock wave position is similar for 4 mm and 5 mm exit diameters and moves slightly upstream for the 6 mm diameter, which results in a considerable drop in critical back pressure.

The other main parameter which strongly affects ejector performance is the nozzle exit position (NEP). NEP is the distance between the primary nozzle exit to the constant area section mixing chamber, relative to the nominal value (with positive values in the downstream direction). Dong et al. [21] and Da-Wen and Eames [22] reported that NEP defines the perfect mixing length of flows inside the mixing chamber which affects the ejector performance. Figure 9(a) shows the effect of NEP on entrainment ratio for two different primary flow temperatures. The static pressure along the center line and the corresponding Mach contours are shown in Fig. 9(b,c). By moving the nozzle upstream ($NEP < 0$) the effective area available for the secondary flow increases, which in turn increases the entrainment ratio (see Fig. 9(a)). However at $NEP = -20$ mm (and a primary flow temperature of 85°C) a further decrease of NEP reduces the entrainment ratio, indicating that the ejector is no longer working in the optimal double-choked regime.

By moving the nozzle upstream from $NEP = 0$ to approximately -20 mm, the second series of oblique shock waves decays and moves towards the mixing chamber inlet. After this point, the second series of shock waves rapidly diminishes which is reflected in a considerable reduction in the amount of entrained flow to the ejector. This reveals the crucial significance of the nozzle exit position parameter on ejector performance and ascertains the necessity of designing a moveable primary nozzle for desired supersonic ejector.

3.2.2.2 *Effect of the mixing chamber geometry*

Ejector performance is strongly dependent on the mixing phenomena inside the mixing chamber. As investigated by Kong et al. [23], both flows should be fully mixed in the mixing chamber to reduce the energy loss in the diffuser section. A good mixing chamber design enhances the tangential-shear interaction between primary and secondary flows with lower loss in the mean kinetic energy of the flow.

Figure 10(a) shows the effect of the mixing chamber diameter d_{mc} on the ejector performance. Decreasing d_{mc} reduces entrainment ratio while the upper limit of back pressure to stay in the double choked flow regime rises. Even though this parameter has no effect on the shape of the primary jet core, smaller mixing chamber diameter restricts the effective area for the secondary flow and reduces the viscous effect and shear mixing between the primary jet core and surrounding entrained flow. As shown in Fig. 10(b), the mixing chamber length l_{mc} does not significantly affect the entrainment ratio. This is because the primary jet core and its expansion angle, plus the effective area of entrained flow do not change for different lengths of mixing chamber. However, this parameter should be within a specific range (here, 30mm to 120 mm), otherwise it will negatively affect the ejector performance due to increased frictional losses.

Figure 10(c) shows the simulated velocity profile distribution at different cross sections inside the ejector. For larger mixing chamber lengths the shear mixing interaction between the two flows increases and the final momentum difference reduces. In Fig. 10(c), the velocity profile at the end of the mixing chamber of 120 mm in length reflects a uniform mixing of primary and entrained flows. Therefore, the second series of shock waves produces lower pressure fluctuations, but also, the strength of the first series of shock waves stays the same for different mixing chamber lengths since these are all coincident at the primary nozzle exit section. Figure 11 shows that the mixing chamber length has no significant influence on the position of the first and second series of shock waves. However, it should be noted that increasing this length increases the pressure drop due to interaction of the flow with the viscous boundary layers. This may deteriorate the ejector performance and negate the benefit of a longer mixing section.

3.2.2.3 *Effect of the diffuser geometry*

Many studies have evaluated the proper range of diffuser expansion angles for a wide range of applications (Banasiaka et al. [24]). Here, the opening angle is fixed at 5 degrees and only the effect of diffuser length has been evaluated. It was found that the ejector length has no significant influence on ejector entrainment ratio. Nonetheless, as with the mixing chamber length (l_{mc}), the diffuser length (l_d) should be chosen from a suitable range which still maintains the ejector performance in the optimum working mode. Very shorter diffuser lengths (in this case, below 30 mm) slightly reduce the critical back pressure.

3.2.3 Dimensional Optimization for a Waste Heat-Driven Vehicle Refrigeration Cycle

In the preceding sections, the effects and optimum ranges of a number of geometrical parameters of the ejector have been assessed independently. For an actual engineering application, such as a vehicle refrigeration system, where the ejector boundary conditions are predefined, it is recommended to use an optimization procedure which considers all the previously mentioned results together.

As an example, the saturation temperatures of primary flow, secondary flow, and downstream exit flow are set at 85°C, 5°C, and 40°C, respectively. The mass flow rate of the secondary flow (\dot{m}_s) is set at 0.0334 kg/s. Starting from the initial values for the ejector dimensions (see Sect. 3.1) and an estimated range for the entrainment ratio ω (see derivation below and Eq. (8)), the main parameters affecting ω are determined: nozzle throat diameter (d_{nt}), nozzle exit diameter (d_{ne}), and mixing chamber diameter (d_{mc}). Next, all the other sizes are selected inside their optimum ranges. Due to the restrictions of the heat exchanger which is used as vapor generator, the estimated range for achievable mass flow rate of primary flow (\dot{m}_p) with a saturation temperature of 85°C using radiator waste heat during normal operation of a vehicle is around 0.133 – 0.222 kg/s. Thus, the estimated range for ω is (Eq. (1)), (see also Alimohammadi et al. [1]):

$$\text{Estimated range of entrainment ratio: } \omega = \frac{\dot{m}_s}{\dot{m}_p} = 0.15 - 0.25 \quad (8)$$

The nozzle throat diameter is adjusted from its initial value (3 mm) to ensure that the mass flow rate of primary flow or entrainment ratio is in the aforementioned range with a saturated exit flow temperature at 40°C (see Table 2). As seen above, the nozzle throat diameters of 4 mm and 4.5 mm are in the calculated range of Eq. (8). Subsequently, for two different nozzle throat diameters (4 mm and 4.5 mm), the mixing chamber diameter and nozzle exit diameter are both adjusted and the resulting entrainment ratios are shown in Table 3 and Table 4, respectively. Empty fields in the tables represent an unacceptable deterioration of performance for this configuration with no flow entrained into the ejector. The maximum entrainment ω is achieved for mixing chamber diameters of 8 mm and 9 mm, and nozzle throat diameters of 4 mm and 4.5 mm, respectively. Table 4 shows that nozzle exit diameters of 6 mm and 6.5 mm are the optimum choice for nozzle throat diameters of 4 mm and 4.5 mm, respectively.

Likewise, all remaining dimensions of the ejector are optimized to achieve the final manufacturing sizes. Note that without sacrificing generality, only integer mm values are considered here for manufacturing simplicity. Typically, from the available optimum combinations which entrain the required mass flow rate from the evaporator, the most lightweight option is selected as optimal geometry:

$$d_{nt} = 4 \text{ mm}, d_{ne} = 6 \text{ mm}, \text{ and } d_{mc} = 8 \text{ mm} \quad (9)$$

with a diffuser exit diameter of at least 15mm, a mixing chamber length between 45mm and 70mm, and a suction chamber curvature of 25mm.

4 Conclusion

In a vehicle cooling system, the compressor of the refrigeration cycle can be replaced by a gas-gas ejector, which receives its energy input from hot water inside the vehicle radiator. The optimum design of ejector is critically important to the coefficient of performance (COP) of the whole system. Due to the high order and complex nature of the flow inside the ejector, it requires a combination of CFD and experimental investigations. An experimental setup is used here to validate the CFD simulation approach, showing a normalized deviation between the observed and simulated results of 5% in terms of the equilibrium pressure.

Using a simple analytical model, the maximum entrainment ratio (ω) has been estimated by correlation of the main influencing parameters in a non-dimensional form. The optimum values of nozzle throat diameter (d_{nt}) and mixing chamber diameter (d_{mc}) are estimated to be used as starting points in the CFD optimization. The developed one-dimensional model can be used in both design and off-design conditions.

Reducing the throat diameter increases the entrainment ratio, but the back pressure should be reduced to maintain the double choked flow regime inside the ejector, which ensures optimum operation. This counteracting effect should be kept in mind in the design of the primary nozzle.

An increase in nozzle exit diameter provides a larger expansion angle and reduces the rate of entrained flow. By variation of nozzle exit diameter, an exact trend for variation of critical back pressure could not be defined from the results. This parameter should be selected using an optimization process which runs the ejector in an acceptable range for the both critical back pressure and entrainment ratio.

The nozzle exit position (NEP) defines the optimal mixing length of the flow in the mixing chamber. This ascertains the necessity of designing a moveable primary nozzle for desired supersonic ejector. The ideal design of the mixing chamber enhances the tangential-shear interaction between primary and secondary flows with lower loss in the mean kinetic energy of the flow. Decreasing the mixing chamber

diameter reduces entrainment ratio, while the upper limit of back pressure to stay in double choked flow regime rises; this diameter does not affect the first series of shock waves. In general, if the mixing chamber diameter is selected larger than its maximum value it causes reverse flow in the ejector whereas if it is chosen too small it destroys the entrainment process. The mixing chamber and diffuser lengths do not significantly affect the entrainment ratio; the resulting velocity profile at the end of a long mixing chamber shows a uniform mixing of primary and entrained flows.

In summary, the paper presents an experimentally validated optimization methodology which accounts for the aforementioned findings in its calculation of the optimal ejector geometry. The final optimized dimensions are reported for a passenger car refrigeration system as a test case; however the approach is generally applicable for the design of ejectors in a wide range of waste heat recovery applications.

Acknowledgements

Dr Tim Persoons is a Marie Curie research fellow of the Irish Research Council (IRC).

References

- [1] Alimohamadi, S., Tehrani, M. S., Farhanieh, B., "Analytical and Numerical Modelling of a Vapor Jet Refrigeration Cycle for Vehicle Air Conditioning," 18th Annual International Conference on Mechanical Engineering-ISME, Tehran, Iran, 2010, Paper No. 2038.
- [2] Riffat, S. B., Everitt, P., "Experimental and CFD Modelling of an Ejector System for Vehicle Air Conditioning," *J. of the Institute of Energy* 72 (1999), 41–47.
- [3] Bartosiewicz, Y., Aidoun, Z., Desevaux, P., Mercadier, Y., "Numerical and Experimental Investigations on Supersonic Ejectors," *Int. J. of Heat and Fluid Flow* 26 (2005), 56-70.
- [4] Sriveerakul, T., Aphornratana, S., Chunnanond, K., "Performance Prediction of Steam Ejector Using Computational Fluid Dynamics: Part 2. Flow Structure of a Steam Ejector Influenced by Operating Pressures and Geometries," *Int. J. of Thermal Sciences* 46 (2007), 823–833.
- [5] Khalil, A., Fatouh, M., Egendyi, E., "Ejector Design and Theoretical Study of R134a Ejector Refrigeration Cycle," *Int. J. of Refrigeration* 34 (2011), 1684–1698.
- [6] Yang, X., Long, X., Yao, X., "Numerical Investigation on the Mixing Process in a Steam Ejector with Different Nozzle Structures," *Int. J. of Thermal Science* 56 (2012), 95-106.
- [7] Aphornratana, S., Eames, I. W., "A small capacity steam-ejector refrigerator: Experimental Investigation of a System Using Ejector with Movable Primary Nozzle," *Int. J. of Refrigeration* 20 (1997), 352–358.
- [8] Lucas, C., Koehler, J., "Experimental Investigation of the COP Improvement of a Refrigeration Cycle by Use of an Ejector," *Int. J. of Refrigeration* 35 (2012), 1595–1603.
- [9] Lucas, C., Koehler, J., Schroeder, A., Tischendorf, C., "Experimentally Validated CO₂ Ejector Operation Characteristic Used in a Numerical Investigation of Ejector Cycle," *Int. J. of Refrigeration* 35 (2012), 1595-1603.

- [10] Tischendorf, C., Lucas, C., Koehler, J., Tegethoff, W., "Visual Investigation of an Ejector Motive Nozzle," Proceedings of the ASME Int. Mechanical Engineering Congress & Exposition, Vancouver, Canada, 2010, Paper No. 38507.
- [11] Rogdakis, E. D., Alexis, G. K., "Design and Parametric Investigation of an Ejector in an Air-Conditioning System," *Int. J. of Applied Thermal Engineering* 20 (2000), 213-226.
- [12] Huang, B. J., Chang, J. M., Petrenko, V. A., Zhunk, K. B., "A Solar Ejector Cooling System Using Refrigerant R141b," *Solar Energy* 64 (1998), 223-226.
- [13] AL-Khalidy, N., Zayonia, A., "Design and Experimental Investigation of an Ejector in an Air-Conditioning and Refrigeration System," *ASHRAE, Trans* 101 (1995), 383-391.
- [14] Hewedy, N. I., Hamed, M. H., Abou-Taleb, F. Sh., Ghonim, T. A., "Optimal Performance and Geometry of Supersonic Ejector," *ASME J. of Fluids Engineering* 130 (2008), 041204-10.
- [15] Kim, S., Kwon, S., "Experimental Determination of Geometric Parameters for an Annular Injection Type Supersonic Ejector," *ASME J. of Fluids Engineering* 128 (2006), 1164-1171.
- [16] Boumaraf, L., Lallemand, A., "Modeling of an Ejector Refrigerating System Operating in Dimensioning and Off-Dimensioning Conditions with the Working Fluids R142b and R600a," *Int. J. of Applied Thermal Engineering* 29 (2009), 265-274.
- [17] Li, C., Li, Y., Wang, L., "Configuration Dependence and Optimization of the Entrainment Performance for Gas-Gas and Gas-Liquid Ejectors," *Int. J. of Applied Thermal Engineering* 48 (2012), 237-248.
- [18] Al-Ansary, H. A., "A Semi-Empirical One-Dimensional Model for Flow in Ejectors Used for Gas Evacuation," Proceedings of ASME 2nd Joint U.S.-European Fluids Engineering Summer Meeting, Miami, Florida, USA, 2006, Paper No. 98138.
- [19] Kim, H. D., Setoguchi, T., Yu, S., Raghunathan, S., "Navier-Stokes Computations of the Supersonic Ejector-Diffuser System with a Second Throat," *Int. J. of Thermal Science* 8 (1999), 79-83.
- [20] Huang, B. J., Chang, J. M., Wang, C. P., Petrenko, V. A., "A 1-D Analysis of Ejector Performance," *Int. J. of Refrigeration* 22 (1999), 354-364.
- [21] Dong, J., Pounds, D. A., Cheng, P., Ma, H. B., "An Experimental Investigation of Steam Ejector Refrigeration Systems," *ASME J. of Thermal Science and Engineering Applications* 4 (2012), 031004.
- [22] Da-Wen, S., Eames, I. W., "Recent Developments in the Design Theories and Applications of Ejectors," *J. of the Institute of Energy* 68 (1995), 65-79.
- [23] Kong, F. S., Kim, H. D., Jin, Y. Z., Setoguchi, T., "Computational Analysis of Mixing Guide Vane Effects on Performance of the Supersonic Ejector-Diffuser System," *Open J. of Fluid Dynamics* 2 (2012), 45-55.
- [24] Banasiaka, K., Hafnerb, A., Andresenb, T., "Experimental and Numerical Investigation of the Influence of the Two-Phase Ejector Geometry on the Performance of the R744 Heat Pump," *Int. J. of Refrigeration* 35 (2012), 1617-1625.

List of Table Captions

Table 1: Result of charging the low pressure tank using ejector for the highest possible charging pressure

Table 2: Optimization of primary nozzle diameter using CFD

Table 3: Optimization of mixing chamber diameter using CFD

Table 4: Optimization of nozzle exit diameter using CFD

List of Figure Captions

Figure 1: Schematic diagram of (a) a vehicle cooling system refrigeration cycle and (b) the ejector

Figure 2: Geometry of solution domain and generated grid for CFD simulation of the ejector

Figure 3: Mach contours of flow in the ejector for an upstream pressure of 27.5 bar, and two downstream pressures (a) 4.8 bar (showing positive outlet flow) and (b) 5.2 bar (showing negative outlet flow)

Figure 4: Variation of the entrainment ratio with area ratio for three different (a) evaporator temperatures (at $T_g = 85^\circ\text{C}$, $T_c = 40^\circ\text{C}$); (b) condenser temperatures (at $T_g = 85^\circ\text{C}$, $T_e = 5^\circ\text{C}$); and (c) generator temperatures (at $T_c = 40^\circ\text{C}$, $T_e = 5^\circ\text{C}$)

Figure 5: Effect on entrainment ratio ω of (a) compression ratio Ψ and driving pressure ratio ξ (for area ratio $\phi = 4.2$) and (b) compression ratio Ψ and area ratio ϕ , for the geometry chosen in sect. 3.1.1 and for saturated generator temperature = 85°C .

Figure 6: (a). Mach contour of flow inside the ejector, (b) pressure distribution of motive and entrained flow along the ejector length

Figure 7: Variation of (a) entrainment ratio with downstream pressure (kPa) and (b) static pressure along the ejector center line ($P_M = 6$ bar), for different nozzle throat diameters ($P_p = 25.26$ bar and $P_s = 3.496$ bar; $d_{nt} = 5$ mm and $d_{mc} = 7$ mm)

Figure 8: Variation of (a) entrainment ratio with downstream pressure (kPa) and (b) static pressure along the ejector center line ($P_M = 6$ bar), for different nozzle exit diameters ($P_p = 25.26$ bar and $P_s = 3.496$ bar; $d_{nt} = 3$ mm and $d_{mc} = 7$ mm)

Figure 9: Effect of nozzle exit position NEP (mm) on (a) entrainment ratio, (b) static pressure along the ejector center line (for $T_p = 85^\circ\text{C}$) and (c) Mach contours ($d_{nt} = 3$ mm, $d_{ne} = 5$ mm and $d_{mc} = 7$ mm)

Figure 10: Effect of (a) mixing chamber diameter (for $l_{mc} = 120$ mm) and (b) length (for $d_{mc} = 7$ mm) on the variation of entrainment ratio with downstream pressure (kPa) ($P_p = 25.26$ bar and $P_s = 3.496$ bar; $d_{nt} = 3$ mm and $d_{ne} = 5$ mm). (c) Velocity profile distribution at different cross sections inside the ejector ($l_{mc} = 120$ mm)

Figure 11: Variation of static pressure along the ejector center line for different mixing chamber lengths ($P_p = 25.26$ bar and $P_s = 3.496$ bar; $d_{nt} = 3$ mm, $d_{ne} = 5$ mm and $d_{mc} = 7$ mm)

List of Tables

Table 1

Upstream pressure (bar)	Maximum downstream pressure (bar)
35	6
27.5	5
19	3.5
15	2.9

Note: Accuracy of pressure gauge sensors is ± 0.3 bar

Table 2

d_{nt} (mm)	3	4	4.5	5
\dot{m}_p (kg/s)	0.098	0.195	0.220	0.499
ω	0.34	0.171	0.152	0.067

Table 3

d_{mc} (mm)	7.5	8	8.5	9	9.5
ω (for d_{nt} of 4mm)	0.174	0.179	×	×	×
ω (for d_{nt} of 4.5mm)	0.034	0.092	0.124	0.166	×

Note: × represents deterioration of ejector performance, with negative flow entrainment

Table 4

d_{ne} (mm)	5	5.5	6	6.5	7	7.5
ω (for d_{nt} of 4mm and d_{mc} of 8mm)	0.179	0.190	0.210	0.183	×	×
ω (for d_{nt} of 4.5mm and d_{mc} of 9mm)	0.166	0.171	0.175	0.188	0.183	0.174

List of Figures

Figure 1

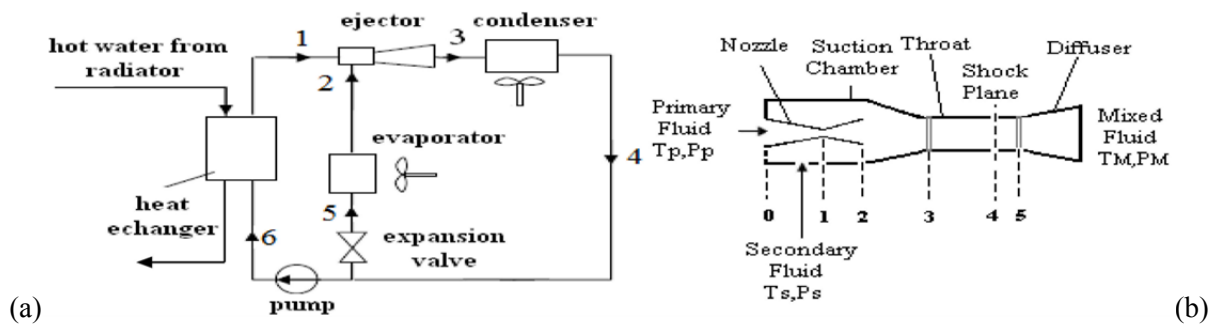


Figure 2

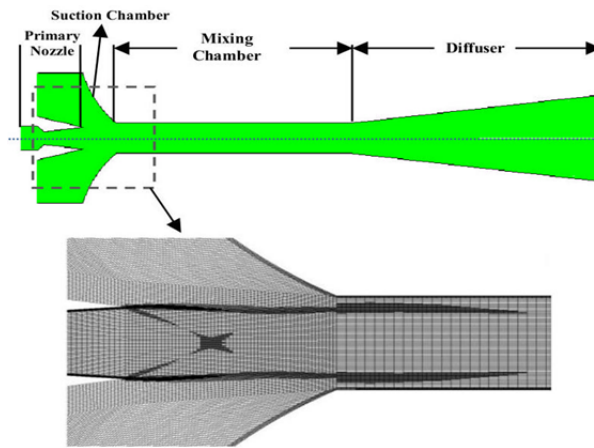


Figure 3

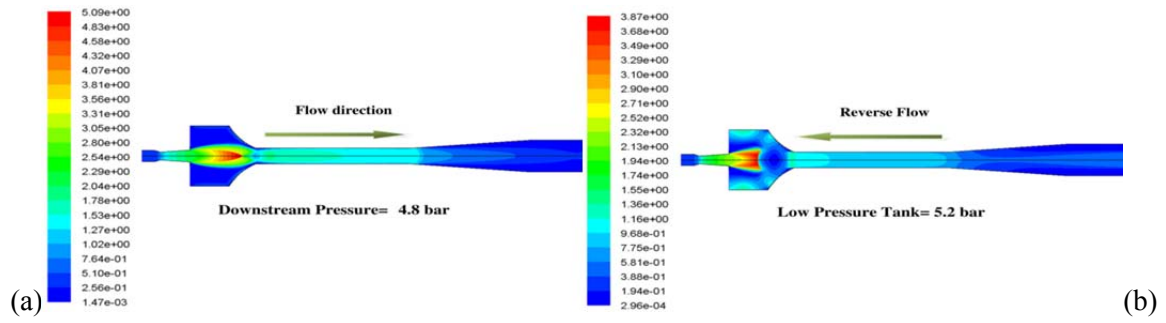


Figure 4

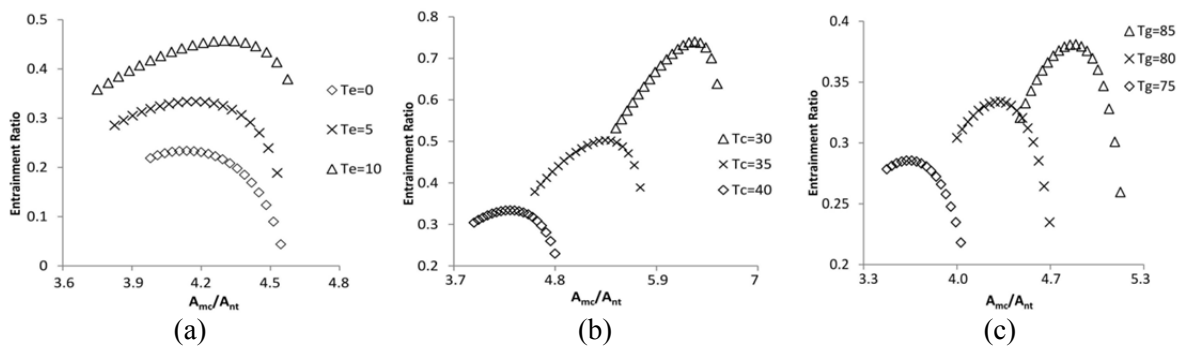


Figure 5

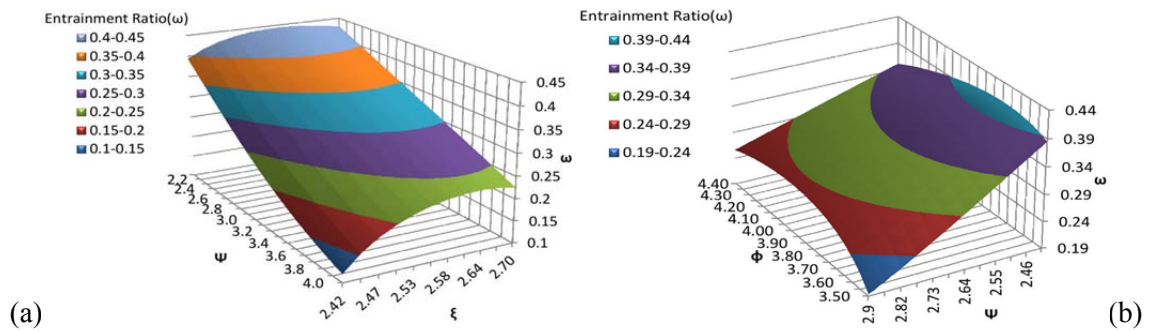


Figure 6

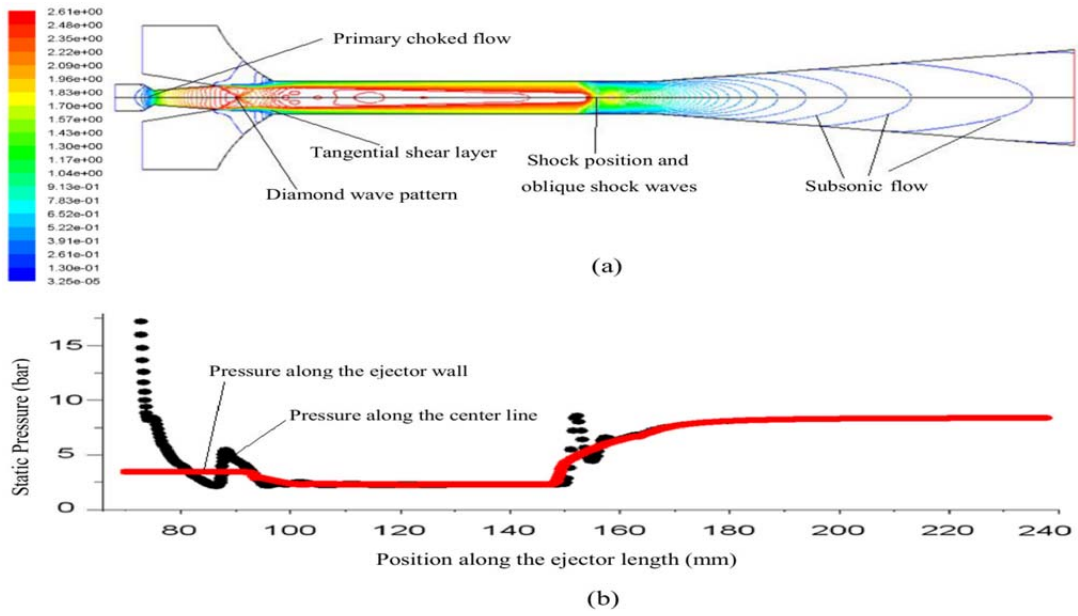


Figure 7

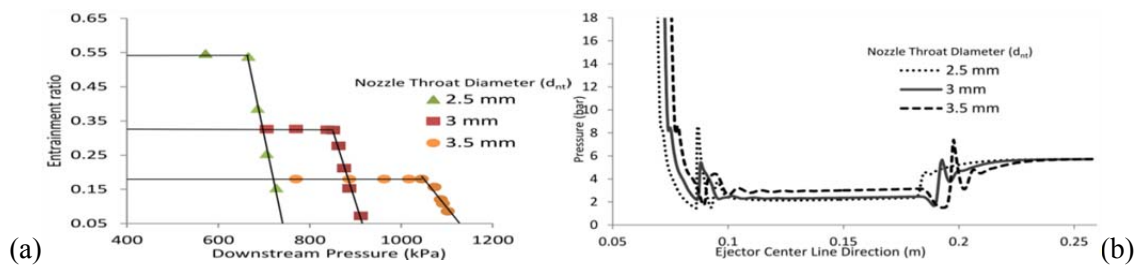


Figure 8

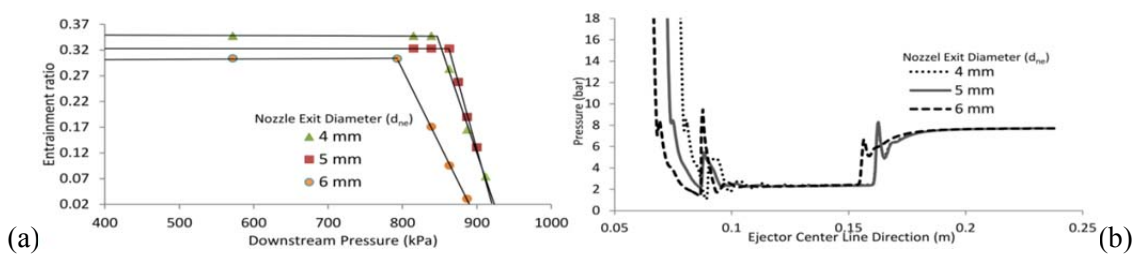


Figure 9

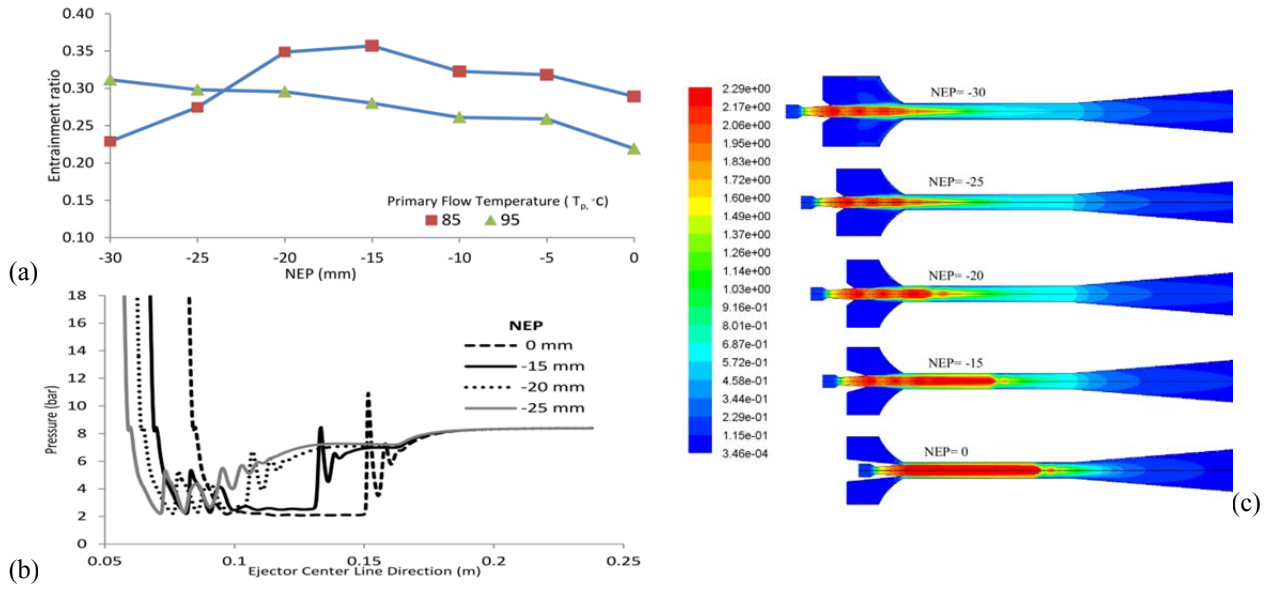


Figure 10

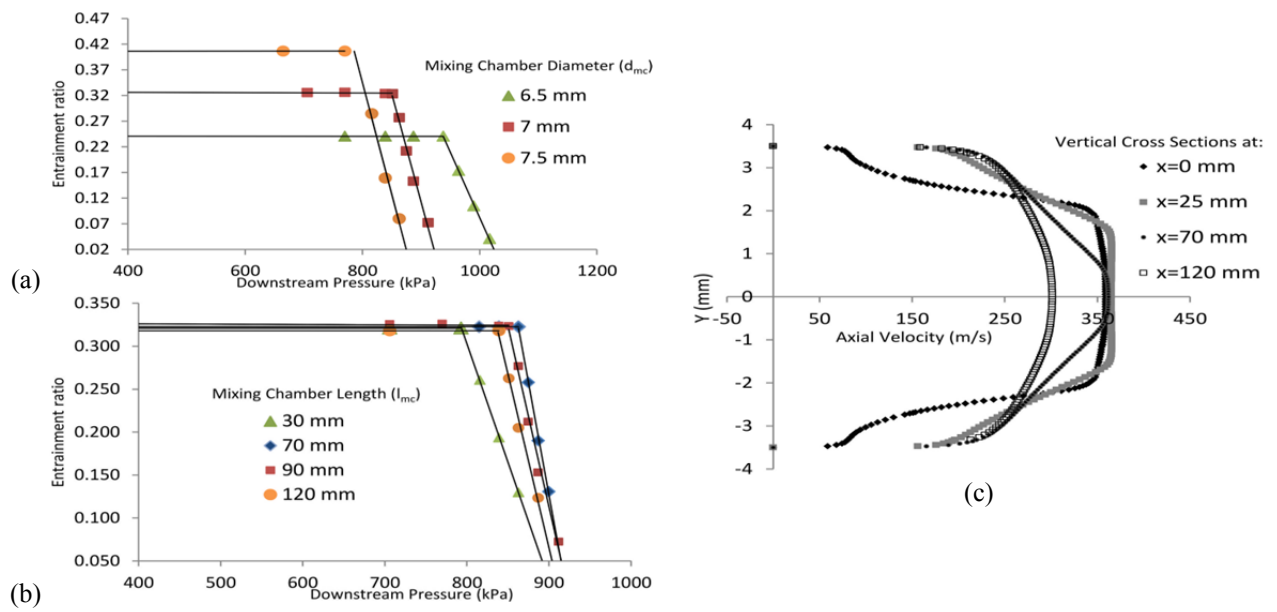


Figure 11

